PNAS
www.pnas.org

Supplementary Information for

Non-steady fracture of transient networks: the case of vitrimer

Tong Shen[1,#], Zhaoqiang Song[3,#], Shengqiang Cai[3,*], Franck J. Vernerey [1,2,*]

1. Department of Mechanical Engineering, University of Colorado Boulder, Boulder, CO, 80302, USA
2. Program of Materials Science and Engineering, University of Colorado Boulder, Boulder, CO, 80302, USA
3. Department of Mechanical and Aerospace Engineering, University of California, San Diego, La Jolla, CA 92093, USA

*Shengqiang Cai, Franck Vernerey
Email: shqcai@ucsd.edu, franck.vernerey@colorado.edu

This PDF file includes:

Supplementary text
Figures S1 to S4 (not allowed for Brief Reports)
SI References

Other supplementary materials for this manuscript include the following:

Movies S1 to S4

Supplementary Information Text

S1. Overview of Transient Network Theory

The rate and history dependent response of materials made of transient network can be captured by the transient network theory developed in our previous works [1–4]. To start, we briefly overview the key concepts of this theory as follows.

The dynamics of chains in the transient network is described by the average rates of bond dissociation (k_d) and reassociation (k_a). During the deformation, the network response is governed by two quantities, the concentration of attached (i.e., mechanically active) chains and their deformation in time. The first quantity can be calculated in time through an evolution equation that captures bond dynamics as [1]:

$$\frac{dn}{dt} = k_a(n_t - n) - k_d n \tag{S1}$$

Where n_t is the total concentration of chains in the network. At chemical equilibrium state ($dn/dt = 0$), the concentration of connected chains becomes a constant and can be found as $n = n_t k_a/(k_a + k_d)$. The second quantity can be described by the so-called chain conformation tensor [1,4] that stores the mean squared stretch of chains in the network:

$$\boldsymbol{\mu} = \langle \boldsymbol{\lambda} \otimes \boldsymbol{\lambda} \rangle \tag{S2}$$

where $\boldsymbol{\lambda}$ is the stretch vector of a chain and the operator $\langle\cdot\rangle$ represents the average over the chain configuration space. With this definition, $\boldsymbol{\mu}$ is equal to identity tensor $\boldsymbol{I}$ when the network is stress-free. Upon deformation, $\boldsymbol{\mu}$ evolves in time according to:

$$\dot{\boldsymbol{\mu}} = \boldsymbol{L}\boldsymbol{\mu} + \boldsymbol{\mu}\boldsymbol{L}^T + k_d(\boldsymbol{\mu_0} - \boldsymbol{\mu}) \tag{S3}$$

Where $\boldsymbol{L} = \dot{\boldsymbol{F}}\boldsymbol{F}^{-1}$is the velocity gradient applied to the network ($\boldsymbol{F}$ being the deformation gradient tensor), $\boldsymbol{\mu}_0 = \frac{3}{tr(\boldsymbol{\mu}^{-1})}\boldsymbol{I}$ is the state at which the chains are associated to. The first two terms on the right-hand side describe the contribution of imposed deformation while the latter two terms account for relaxation of $\boldsymbol{\mu}$ due to bond dynamics. For a purely elastic network (i.e., $k_a = k_d = 0$), $\boldsymbol{\mu}$ degenerates to the Finger tensor $\boldsymbol{\mu} = \boldsymbol{F}\boldsymbol{F}^T$ and eq.4 describes its objective Truesdell rate $\hat{\boldsymbol{\mu}} = \dot{\boldsymbol{\mu}} - \boldsymbol{L}\boldsymbol{\mu} - \boldsymbol{\mu}\boldsymbol{L}^T = \boldsymbol{0}$ [5]. Since $\boldsymbol{\mu}$ stores information about the network elastic deformation, it is directly related to the elastic energy density ψ and the rate of energy dissipation $\mathcal{D}$. Assuming Gaussian chains (i.e., the force-stretch relation of a chain is linear), these two quantities are calculated as [1]

$$\psi = \frac{nk_BT}{2} tr(\boldsymbol{\mu} - \boldsymbol{I}) + p(\det(\boldsymbol{F}) - 1) \quad \text{and} \quad \mathcal{D} = k_d\psi \tag{S4}$$

where p is the hydrostatic pressure that enforces incompressibility. The expression for $\mathcal{D}$ quantifies the loss of strain energy due to chain dissociation. Finally, the Cauchy stress tensor $\boldsymbol{\sigma}$ is finally given by:

$$\boldsymbol{\sigma} = nk_BT(\boldsymbol{\mu} - \boldsymbol{I}) + p\boldsymbol{I} \tag{S5}$$

Due to the chain dynamics, the network deformation may not coincide with the macroscopic deformation of the specimen. This indicates a permanent deformation of the specimen after a loading-unloading cycle. Therefore, the specimen deformation (measured by the deformation gradient tensor $\boldsymbol{F}$) can be split into two parts, a purely dissipative component $\boldsymbol{F}_d$ and a purely elastic deformation $\boldsymbol{F}_e$ [6,7]. According to the multiplicative decomposition, $\boldsymbol{F}_d$ describes the evolution of the reference configuration while $\boldsymbol{F}_e$ is related to the network elastic deformation (related to $\boldsymbol{\mu}$). In summary, we have the following relation:

$$\boldsymbol{F} = \boldsymbol{F}_e\boldsymbol{F}_d \quad \text{and} \quad \boldsymbol{\mu} = \boldsymbol{F}_e\boldsymbol{F}_e^T \tag{S6}$$

For pure shear extension experiment, we can therefore decompose the vertical stretch λ into an elastic and dissipative component as $\lambda = \lambda_e\lambda_d$ where $\lambda_e = \sqrt{\mu_{22}}$.

In pure shear experiment, the conformation tensor reads $\boldsymbol{\mu} = diag(1, \lambda_e^2, 1/\lambda_e^2)$. Along the vertical direction, the evolution equation then reads $\dot{\mu}_{22} = \frac{d}{dt}(\lambda_e^2) = 2\dot{\epsilon}\lambda_e^2 + k_d\left(\frac{3}{\lambda_e^2 + 1/\lambda_e^2} - \lambda_e^2\right)$. Reorganizing this equation, we get the evolution of $\dot{\lambda_e}$ as

$$\dot{\lambda}_e = \frac{\lambda_e k_d}{2}\left(2W + \frac{3}{1+\lambda_e^4} - 1\right) \tag{S7}$$

which is eq. 1a in main manuscript. Furthermore, the evolution of ψ follows $\dot{\psi} = \frac{s}{2}(\boldsymbol{\mu}\colon \boldsymbol{L}) - k_d(\psi - \psi_0)$. Using $\boldsymbol{\mu} = diag(1, \lambda_e^2, 1/\lambda_e^2)$ and $\boldsymbol{L} = diag(0, \dot{\epsilon}, -\dot{\epsilon})$, one can obtain eq. 1b in the main manuscript as:

$$\dot{\psi} = \frac{sk_d}{2}\left[2W\left(\lambda_e^2 - \frac{1}{\lambda_e^2}\right) - \psi\right] \tag{S8}$$

Figure S2 plots the evolution of λ_e as a function of specimen stretch H/H_0 for four different loading rates used in fracture experiment. We see that for the fastest loading ($W_0 = 0.6$), maximum stretch of the network is about λ_e.

Calculation of crack driving force

The crack driving force $\mathcal{G}$ is defined as the decrease of strain energy per increase in fracture surface area. In this work, we consider a pure-shear specimen with a cut of length c (Figure S6) being elongated at a strain rate $\dot{\epsilon}$. To obtain the crack driving force, let us consider the cut extends by a small increment δ_c with velocity $\dot{c}$ during a small time interval δt. Ignoring the inertial effect, the conservation of energy during this process follows:

$$\delta\Pi_w = \delta\Pi_e + \delta\Pi_\mathrm{d} + \delta\Pi_c \tag{S9}$$

where $\delta\Pi_w$ is the work done by external load, $\delta\Pi_e$ is the change of stored elastic energy, $\delta\Pi_d$ is the energy dissipated by bulk relaxation and $\delta\Pi_c$ is the energy flows to the crack. The crack driving force $\mathcal{G}$ is then computed as

$$\mathcal{G} = \lim_{\delta c \to 0}\frac{\delta\Pi_c}{\delta c} = \lim_{\delta c \to 0}\left[\frac{1}{\delta c}(\delta\Pi_w - \delta\Pi_e - \delta\Pi_\mathrm{d})\right] \tag{S10}$$

These quantities Π_w, $\delta\Pi_e$ and $\delta\Pi_\mathrm{d}$ are calculated based on the specimen evolution from state *a* to *b* as follows. First, the work of external load is calculated from the boundary traction $\bar{\boldsymbol{\tau}}$ and velocity $\boldsymbol{v}$ as $\delta\Pi_w = \int_{\delta t}\int_{\mathcal{S}} \bar{\boldsymbol{\tau}} \cdot \boldsymbol{v}\, \mathrm{d}\mathcal{S}\ dt$, where $\mathcal{S}$ is the top and bottom boundary of the specimen. Applying the divergence theorem, this integral can be converted into a volume integral over the specimen as:

$$\delta\Pi_w = \int_{\delta t}\int_V \boldsymbol{\sigma}\colon \boldsymbol{L}\, dV\, dt \tag{S11}$$

The change of stored elastic energy $\delta\Pi_e$ is evaluated as:

$$\delta\Pi_e = \int_{\delta t}\int_V \dot{\psi}\, dV\, dt \tag{S12}$$

Lastly, the energy dissipated by bulk relaxation is calculated as:

$$\delta\Pi_d = \int_{\delta t}\int_V k_d\psi\, dV\, dt \tag{S13}$$

Once eq. S9-S11 are evaluated, one can determine the crack driving force via eq. S8. For general problems, this usually require numerical simulations due to the complexity in geometry. An example can be found in our previous work [8] where a finite element numerical scheme is used to simulate the pure shear fracture. In the next section, we will briefly introduce this framework and show how it describes our experimental results.

S2. Finite element modeling of pure shear fracture

The finite element scheme is developed in our previous work [8] using a customized program written in Matlab. Figure S5 shows an example of numerical simulation, where only the top half of a shear crack sample is included due to the problem symmetry. The bottom boundary is divided into two parts, the traction free section of length c_0 (crack surface) and a "solid" section whose vertical motion is constrained. When the crack is unstable, these vertical constraints are removed sequentially to create new crack surfaces. The model dimension is set according to the experimental condition. All material parameters (force sensitivity f_0, crosslink density n, natural bond dissociation rate k_d^0) are calibrated via relaxation experiments in our previous work [9].The chain stiffness k is calculated by assuming Gaussian chains $k = 3k_BT/\sqrt{N}b$ where k_BT is the thermal energy, N is the chain length and b is the segment length. β is treated as a fitting parameter, whose physical meaning is related to both the average energy threshold of chain damage and the size of damage zone ahead of the tip. In this work, β is calibrated as $73\ J$. Figure S5c and d show the matching between the model prediction and experiment corresponding to the cases shown in Fig.1. The solid lines are model predictions and scattered symbols are experimental measurements.

S3. Analytical derivation of $\mathcal{G}$

The analytical approximation of $\mathcal{G}$ can be obtained by considering the specimen at its reference configuration (Figure S6a) whose height H^a is related to the deformed height H as $H^a = H/\sqrt{\mu_{22}}$. To simplify the problem, we made two assumptions similar to the derivation of Griffith [10] and Rivlin [11]. First, the stress distribution is approximated by a binary field where there is an unloaded zone behind the tip (the grey region in Figure S6a) and a uniformly deformed zone ahead of the tip, whose stored elastic energy density ψ equals to the one in the far field. Second, we assume that the notch tip remains sharp during the deformation. Under these two assumptions, the effect of crack propagation is to unload a strip of loaded material (the orange region in Figure S6b) due to the advancement of the notch tip. Therefore, eq. S9-S11 can be evaluated by an imaginary process of the specimen evolving from state *a* to *b*, during which the notch extends by δc with velocity $\dot{c}$ ($\delta c = \dot{c}\delta t$).

Due to the simplicity in geometry, eq. S9-S11 can be evaluated by directly comparing the geometry and stress states between *a* and *b*. Further invoking the linear approximation of stored elastic energy $\psi^b = \psi^a + \dot{\psi}\delta t + \mathcal{O}(\delta t^2)$ and the volume of loaded zone $V_b = V_a + \dot{V}\delta t + \mathcal{O}(\delta t^2)$, $\delta\Pi_w$, $\delta\Pi_e$ and $\delta\Pi_d$ are evaluated as:

$$\begin{aligned} \delta\Pi_w &= \int_{V_a} \boldsymbol{\sigma}\colon \boldsymbol{L}\, dV\ \delta t + \mathcal{O}(\delta t^2) \\ \delta\Pi_e &= \int_{V_b} \psi^b\, dV - \int_{V_a} \psi^a\, dV + \mathcal{O}(\delta t^2) \\ \delta\Pi_d &= \int_{V_a} k_d\psi^a\, dV\ \delta t + \mathcal{O}(\delta t^2) \end{aligned} \tag{S13}$$

Plugging eq. S12 into eq. S8, the crack driving force $\mathcal{G}$ is obtained as $\mathcal{G} = \lim_{\delta c\to 0}\frac{1}{\delta c}\int_{V_b-V_a}\psi^a\, dV = \psi^a H^a + \mathcal{O}(\delta t)$. Further recalling that $H^a = H/\sqrt{\mu_{22}}$ where H is the specimen's height at deformed state, we obtain:

$$\mathcal{G} = \frac{H}{\sqrt{\mu_{22}}}\psi \tag{S14}$$

Where we omit the superscript "α" for H and ψ to be consistent with the main paper.

Reference

1. Vernerey, F. J., Long, R. & Brighenti, R. A statistically-based continuum theory for polymers with transient networks. *J. Mech. Phys. Solids* **107**, 1–20 (2017).
2. Lalitha Sridhar, S. & Vernerey, F. J. The Chain Distribution Tensor: Linking Nonlinear Rheology and Chain Anisotropy in Transient Polymers. *Polymers* **10**, 848 (2018).
3. Shen, T., Long, R. & Vernerey, F. Computational modeling of the large deformation and flow of viscoelastic polymers. *Comput. Mech.* 1–21 (2018) doi:10.1007/s00466-018-1619-0.
4. Shen, T. & Vernerey, F. Rate-dependent Fracture in Transient Networks. *J. Mech. Phys. Solids*.
5. Wiley: Nonlinear Solid Mechanics: A Continuum Approach for Engineering - Gerhard A. Holzapfel. http://www.wiley.com/WileyCDA/WileyTitle/productCd-0471823198.html.
6. Lubliner, J. A model of rubber viscoelasticity. *Mech. Res. Commun.* **12**, 93–99 (1985).
7. Saxena, P., Hossain, M. & Steinmann, P. A theory of finite deformation magneto-viscoelasticity. *Int. J. Solids Struct.* **50**, 3886–3897 (2013).
8. Shen, T. & Vernerey, F. J. Rate-dependent fracture of transient networks. *J. Mech. Phys. Solids* **143**, 104028 (2020).
9. Song, Z., Shen, T., Vernerey, F. & Cai, S. Force-dependent bond dissociation explains the rate- dependent fracture of vitrimers. *Rev.*
10. Griffith, A. A. & Taylor, G. I. VI. The phenomena of rupture and flow in solids. *Philos. Trans. R. Soc. Lond. Ser. Contain. Pap. Math. Phys. Character* **221**, 163–198 (1921).
11. Rivlin, R. S. & Thomas, A. G. Rupture of Rubber. I. Characteristic Energy for Tearing. in *Collected Papers of R.S. Rivlin: Volume I and II* (eds. Barenblatt, G. I. & Joseph, D. D.) 2615–2642 (Springer, 1997). doi:10.1007/978-1-4612-2416-7_180.

Fig. S1.

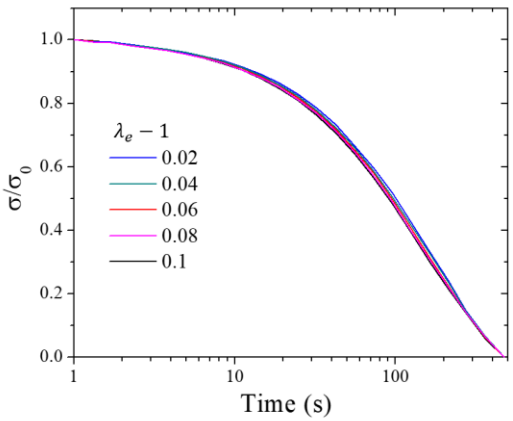

Figure S1. Stress relaxation experiment at different strain λ_e with uniaxial tensile loading for small deformation ($\lambda_e < 1.1$).

Fig. S2.

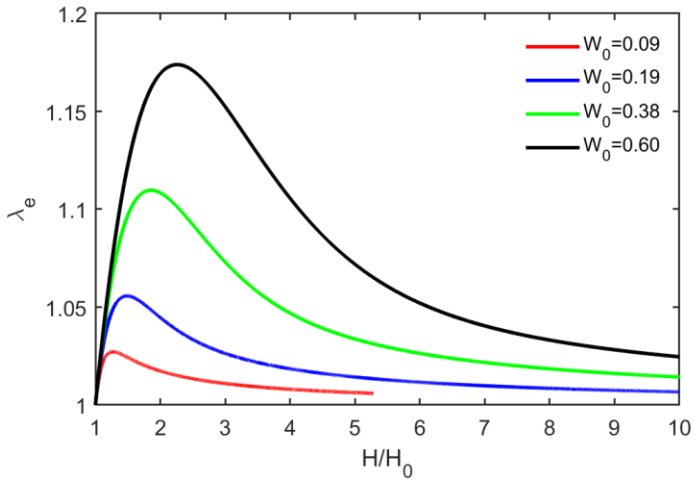

Figure S2. Evolution of average chain stretch λ_e as a function of specimen stretch H/H_0 for four different loading rates conducted in fracture experiment

Fig. S3.

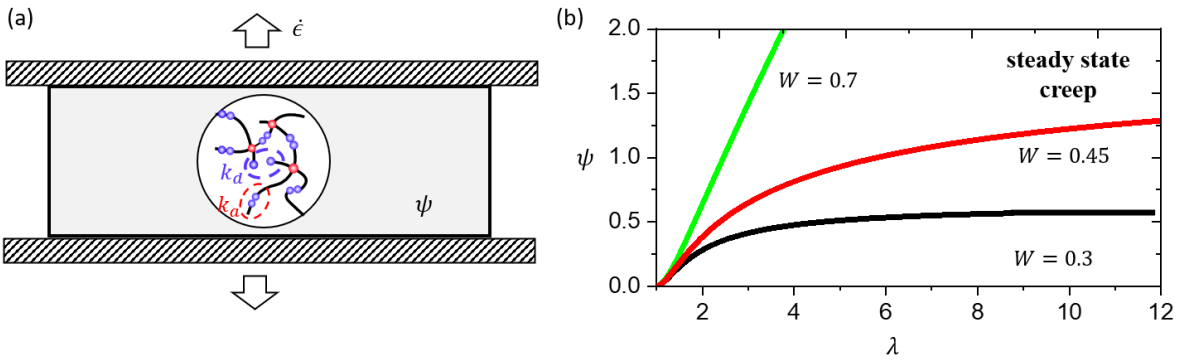

Figure S3. When elongating a specimen at constant true strain rate, the stored elastic energy density $\boldsymbol{\psi}$ increases to a plateau value (characterizing the steady state creep condition) when $\boldsymbol{W < 0.5}$. When $\boldsymbol{W >}$ $\boldsymbol{0.5}$, $\boldsymbol{\psi}$ increases without bound.

Fig. S4

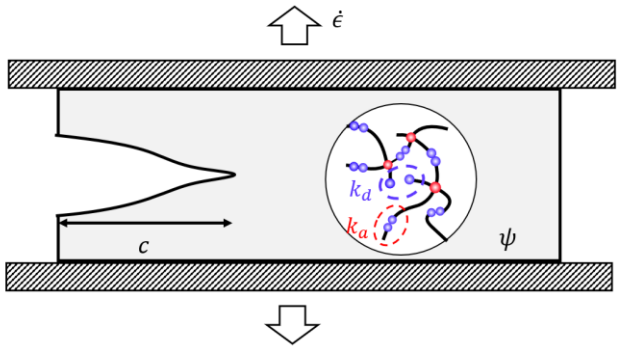

Figure S4 Schematic of a fractured pure-shear specimen made of transient network.

Fig. S5

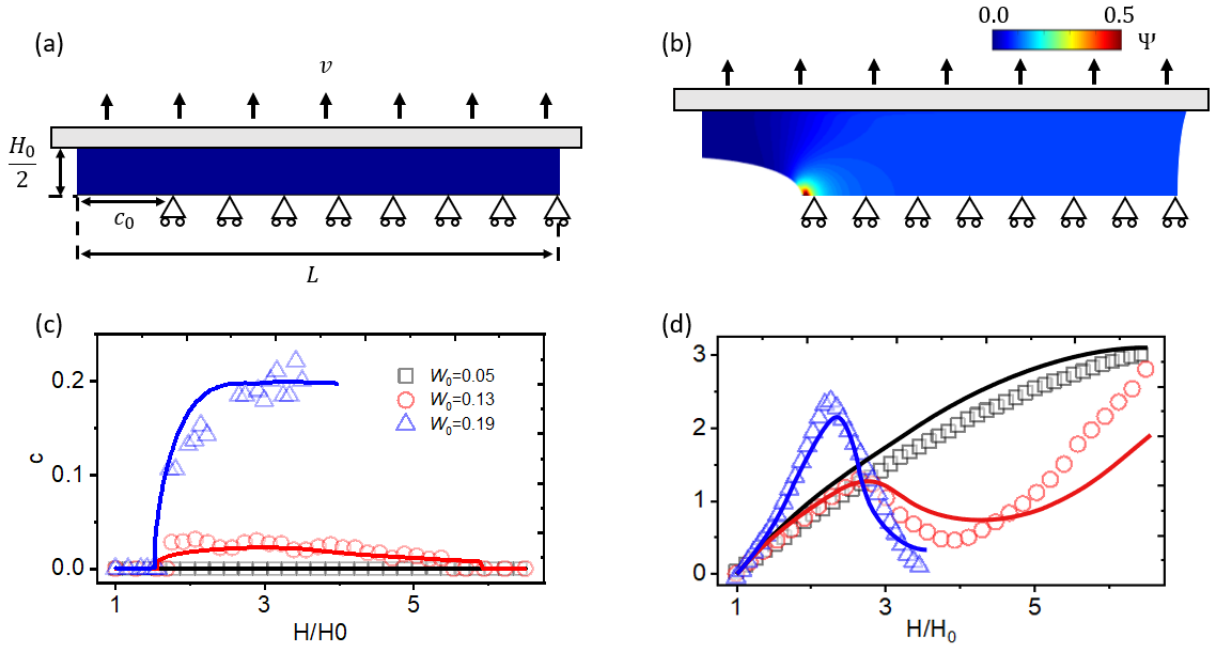

Figure S5. Example of the finite element simulation and boundary condition for (a) the undeformed state and (b) deformed state. (c) The maching between simulation and experiment on crack velocity $\dot{c}$. (d) The maching between simulatio nand experiment on crack opening angle θ.

Fig. S6

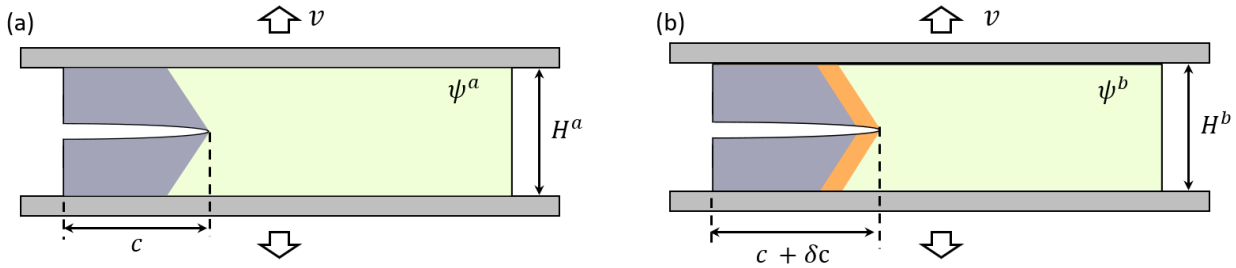

Figure S6. Schematic of simplified stress field in a pure-shear sample (a) before and (b) after a crack propagates by a small increment δc

Fig. S7

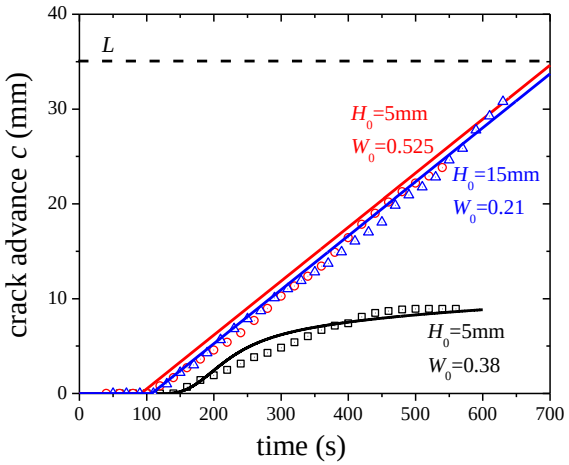

Figure S7, comparison between crack extension c as a function of time for different specimen thicknesses. The scatter symbols are experimental measurement and the solid lines are model prediction.

SI Video1. Animation of experiment and simulation on $H_0 = 10\ mm$ and $W_0 = 0.065$.
SI Video2. Animation of experiment and simulation on $H_0 = 10\ mm$ and $W_0 = 0.13$.
SI Video3. Animation of experiment and simulation on $H_0 = 10\ mm$ and $W_0 = 0.26$.
SI Video4. Animation of experiment and simulation on $H_0 = 10\ mm$ and W_0. Varies in time follow the relation show in Figure. 5A.